



Contents lists available at ScienceDirect

International Journal of Applied Earth Observation and Geoinformation

journal homepage: www.elsevier.com/locate/jag



GOCE gravity gradient data for lithospheric modeling

Johannes Bouman ^{a,*}, Jörg Ebbing ^{b,c}, Sjef Meekes ^d, Rader Abdul Fattah ^d, Martin Fuchs ^a, Sofie Gradmann ^b, Roger Haagmans ^e, Verena Lieb ^a, Michael Schmidt ^a, Denise Dettmering ^a, Wolfgang Bosch ^a

^a Deutsches Geodätisches Forschungsinstitut (DGFI), Alfonz-Goppel-Str. 11, D-80539 Munich, Germany

^b Geological Survey of Norway (NGU), Leiv Eirikssons vei 39, 7491 Trondheim, Norway

^c Norwegian University of Science and Technology, 7491 Trondheim, Norway

^d TNO, Princetonlaan 6, 3584 CB Utrecht, The Netherlands

^e ESA/ESTEC, Keplerlaan 1, 2201 AZ Noordwijk, The Netherlands

ARTICLE INFO

Article history:

Received 17 May 2013

Accepted 1 November 2013

Keywords:

GOCE gravity gradients

Lithosphere

Moho

Heat flow determination

ABSTRACT

The Gravity field and steady-state Ocean Circulation Explorer (GOCE) is the European Space Agency's (ESA) satellite gravity mission to determine the Earth's mean gravity field. GOCE delivers gravity gradients, a new type of satellite data. We study how these data can improve modeling of the Earth's lithosphere. We discuss the use of the original GOCE gravity gradients versus the use of gravity gradients in grids at satellite altitude or close the Earth's surface and conclude that grids are easier to handle than the original data because one does not have to deal with very different error characteristics of the different gradients, given in a rotating frame at varying heights. The downward continuation to the surface enhances signal and better reflects the near-surface geology. But this does not outweigh the amplification of noise and omission errors, which is why we recommend using the field at mean satellite altitude for lithospheric modeling. The North-East Atlantic region is ideal to analyze the additional value of GOCE gravity gradients because it is a well-studied region in terms of regional geophysics. We calculated the gradient sensitivity for crustal depth slices using a 3D lithospheric model. This reveals that especially interfaces with large density contrasts have a distinct signal in the gravity gradients, but that they are quite insensitive to intra-crustal density sources, which can have quite a large effect on surface gravity data. We also show that the satellite gradients have a depth sensitivity well suited to study the upper mantle density structure, making them complementary to gravity and seismic tomography. In the underexplored Rub'al-Khali area the GOCE vertical gradient was used to invert for crustal thickness. The updated Moho model gives a good fit to four of the six gradients and independent depths from seismic stations. The Moho model was used to update the heat flow model and source rock maturity maps, which are generally consistent with known source rock maturity trends in the surrounding regions. GOCE gradients are therefore useful to map crustal thickness and deep regional structures for frontier areas. In combination with other data, heat flow can be modeled which is essential for basin maturity evaluation.

© 2013 Elsevier B.V. All rights reserved.

1. Introduction

GOCE is ESA's satellite mission that combines gravity gradiometry and GPS tracking to determine the Earth's mean gravity field with unprecedented, global accuracy and a spatial resolution up to 80 km (ESA, 1999). We explore how GOCE gravity gradient¹ data can improve modeling of the Earth's lithosphere and thereby

contribute to a better understanding of Earth's dynamic processes. To this end, we study the sensitivity of this new type of satellite data to lithospheric density structure in the well explored and understood North-East Atlantic Margin. We assess the sensitivity of the GOCE gravity gradient data to geological structures with respect to their depth and relative density contrast. This analysis provides improved information about the lithosphere compared with results obtained by other more common sources like terrestrial gravity data, and seismic.

The obtained knowledge is transferred to a second study area, which is an underexplored region: the Rub'al-Khali desert on the Arabian Peninsula. Here gravity gradient data will be used to update a presumably less accurate geological model of the basin thickness, with the goal to improve the modeling for hydrocarbon exploration

* Corresponding author. Tel.: +49 89230311114.

E-mail address: bouman@dgfi.badw.de (J. Bouman).

¹ Strictly speaking GOCE delivers gravitational gradients as there is only gravitation acting on the satellite but no force caused by Earth rotation. We stick here to the commonly used term gravity gradients.

purposes. An updated Moho model – based on GOCE gradients – is validated with measured depths at a few available seismic stations. In addition, we discuss the updated heat flow model that was created with the new Moho model as input.

The use of GOCE gravity gradient data, however, is not straightforward for a number of reasons. First of all, the gradients are given in a rotating instrument frame. Secondly, four of the six measured gradients are much more accurate than the remaining two. In addition, the gradients have their highest accuracy in the measurement bandwidth (MBW) between 5 mHz and 100 mHz, with increasing errors above and below the MBW. These error characteristics hinder the rotation of the gradients from the instrument frame to reference frames directly related to the Earth. We will therefore address the direct use of the gradients and compare this with using gradient grids at mean satellite altitude as well as grids close to the Earth's surface.

Our paper is organized as follows. In Section 2 we discuss in some detail the error characteristics of the GOCE gradients and review the different options to use the contained gravity field information. The case study for the North-East Atlantic margin is presented in Section 3 and the transfer to Rub'al-Khali in Section 4. Finally, Section 5 contains the conclusions.

2. GOCE data and their preparation for geophysical studies

2.1. Characteristics of GOCE gravity gradient data

The GOCE gravity gradient data are delivered by the on-board gradiometer. The gradients are not directly measured, but derived from the differences between the accelerations of three pairs of accelerometers (Frommknecht et al., 2011). The gradiometer configuration is such that the V_{XX} , V_{YY} , V_{ZZ} and V_{XZ} gradients are determined with high accuracy, whereas the V_{XY} and V_{YZ} gradients are less accurate. Here (X , Y , Z) forms the gradiometer reference frame (GRF), which co-rotates with the satellite. The drag free and attitude control system (DFACS) keeps the X -axis as good as possible aligned with the velocity vector of the satellite minimizing drag, the Y -axis is perpendicular to the orbital plane and the Z -axis points in almost radial direction. The gradients obtain their highest accuracy in the MBW, which roughly corresponds to an along-track spatial resolution of 750–40 km. The current effective spatial resolution of GOCE data is around 90 km at the Earth's surface as we will see below.

Although GOCE has a near circular orbit, the height above the Earth's surface varies because of orbit resonances and because the Earth is not a sphere. This is demonstrated in Fig. 1, which displays the height of the satellite as a function of latitude for one repeat cycle of the nominal mission (61 days). One sees that the perigee height is 255 km, but for high latitudes the height above the Earth's surface increases. The mean height above the ellipsoid is 270 km.

2.2. Derived gravity field products

The GOCE gravity gradients in the GRF are used to compute GOCE-based global gravity field models (e.g. Pail et al., 2011). Commonly these global models use a spherical harmonic expansion up to degree and order 250. EGM2008 is a high-resolution global gravity field model up to degree 2190, which combines information from the satellite gravity mission GRACE, terrestrial gravity data and satellite altimeter data (Pavlis et al., 2012). The added value of GOCE becomes clear when comparing GOCE-based models with existing models that include terrestrial gravity data. The latter data may be of poor quality or absent in certain regions of the world, and models such as EGM2008 may suffer. This is shown in Fig. 2 displaying the gravity anomaly differences between GOCO03S

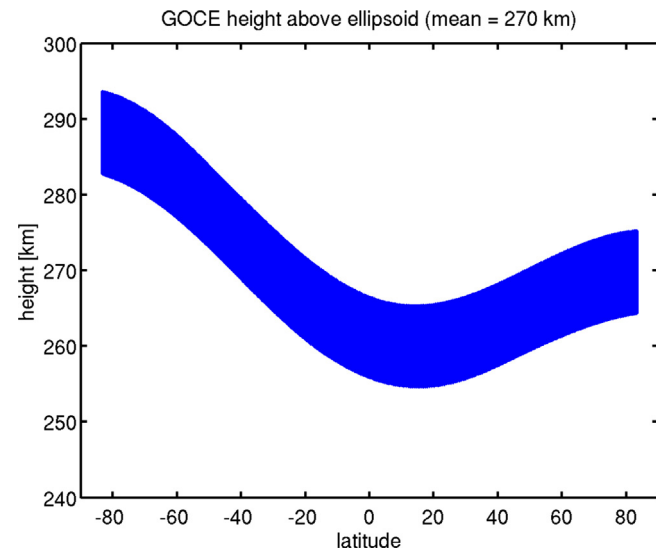


Fig. 1. Height of the GOCE satellite above the ellipsoid as a function of latitude.

(Mayer-Gürr et al., 2012) and EGM2008 up to spherical harmonic degree and order 200. For our North-East Atlantic study area with high quality terrestrial data the differences are smaller than for the study area in Saudi Arabia where the quality of the terrestrial gravity data in EGM2008 may be less. For global comparisons see Bouman et al. (2011) and Bouman and Fuchs (2012).

The latest GOCE global gravity field models represent the original gravity gradient data well (Bouman and Fuchs, 2012). These models also allow synthesizing arbitrary functionals of the gravitational potential everywhere on or above the Earth's surface. Nevertheless, there are a number of reasons why one may not like to use these global models. First of all, it may be more convenient to use gravity gradients instead of a set of spherical harmonic coefficients. Secondly, the global gravity field models are regularized and/or use a priori information. Because the models are global, the regularization is global as well. This may, however, not be optimal for all regions and dedicated regional gravity field solutions seem to be able to extract more signal from the GOCE data (Schall et al., 2012). One may therefore prefer to directly use the gradients.

The original GOCE gradients, however, are given in the GRF, which is a rotating instrument frame. In addition, 4 of the 6 gradients are accurate in the MBW. Above and below the MBW the gradients are less accurate and may contain systematic errors. The two less accurate gradients V_{XY} and V_{YZ} have errors that are about two orders worse than the accurate gradients V_{XX} , V_{YY} , V_{ZZ} and V_{XZ} . Thus it is not straightforward to use the gradients in the GRF. Alternatively, gradients in the Local North-Oriented Frame (LNOF) are given (Bouman et al., 2009, 2011; Fuchs and Bouman, 2011). These gradients are rotated to the LNOF after replacement of the long wavelength signal below the MBW with gradients from a global gravity field model. Also V_{XY} and V_{YZ} are computed from such a model. The LNOF gradients are a compromise between easier to use and keeping as much as possible the original GOCE data.

The GRF and LNOF gradients are given along the orbit, with varying height. An alternative representation therefore is in grids at a mean altitude. On the one hand the computation of grids averages out noise and on the other hand a regular grid at one altitude is more straightforward to handle than the gradients along the orbit. One could use grids at mean orbit altitude or one could downward continue to, for example, 10 km above the Earth's surface (Fig. 3). Downward continuation amplifies signal, but also amplifies noise (see Table 1). It also has to be noted that the spatial resolution at which the noise becomes larger than the signal does not change

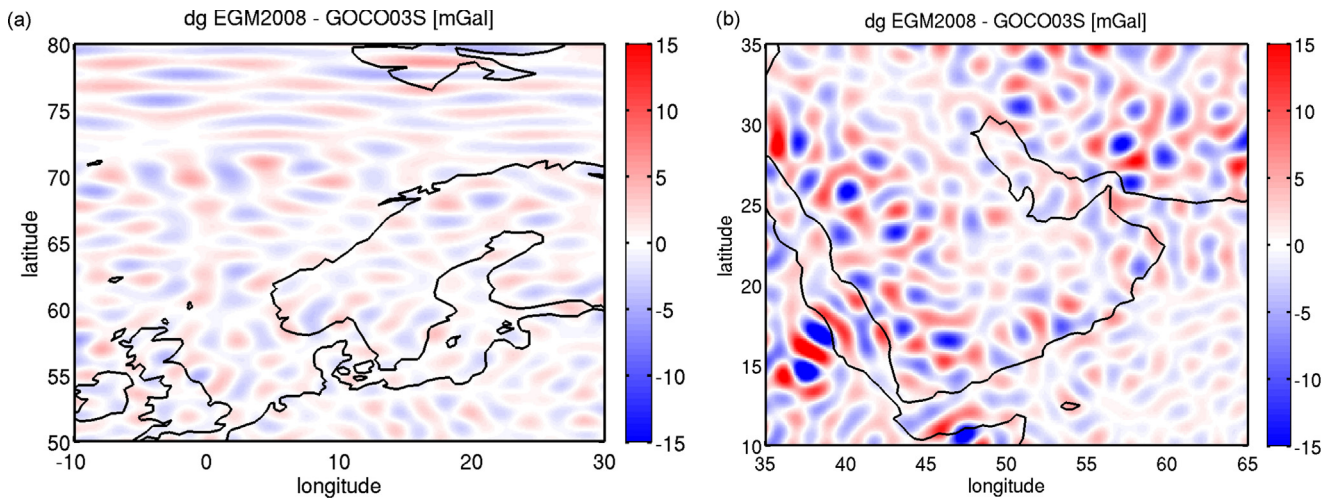


Fig. 2. Gravity anomaly differences at the Earth's surface between EGM2008 and GOCO03S in northern Europe (a) and the Arabian Peninsula (b). Both models were evaluated up to spherical harmonic degree and order 200.

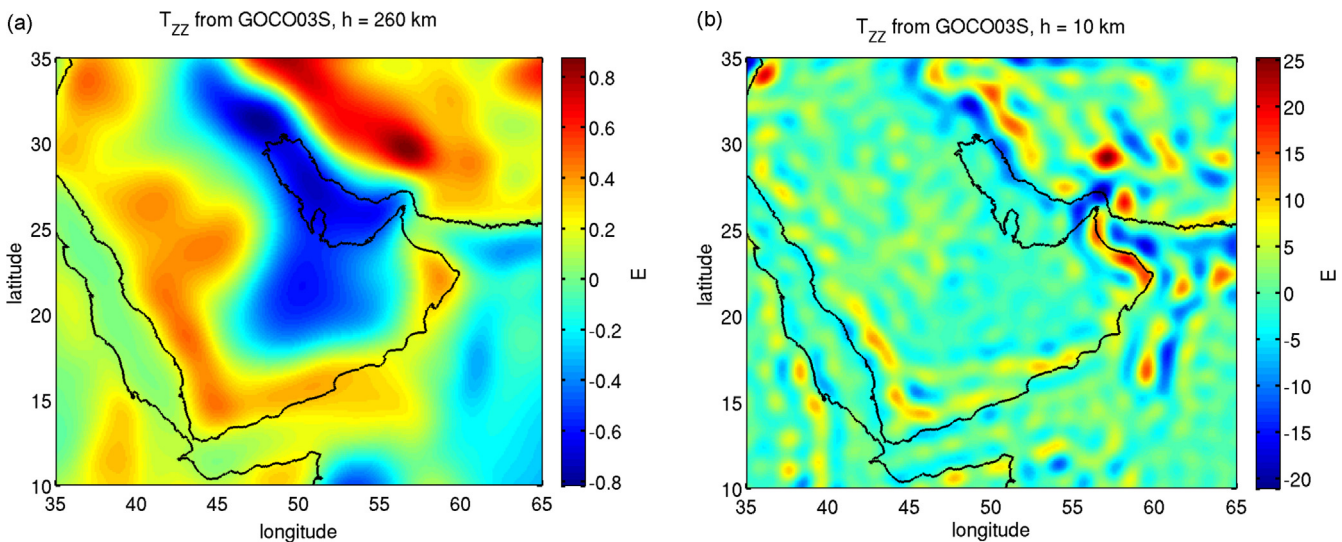


Fig. 3. Vertical gravity gradient for the Arabian Peninsula from GOCO03S at satellite height (a) and 10 km above the Earth's surface (b). The GOCO03S model was used complete to spherical harmonic degree and order 250. Units are Eötvös, $1 \text{ E} = 10^{-9} \text{ s}^{-2}$.

through downward continuation (see Fig. 4). What does change, however, is the omission error. At satellite altitude the high frequency signal is damped more than at 10 km altitude. In other words, the total signal power above the GOCE resolution is relatively less at satellite altitude, whereas it is large close to the Earth's surface. Going to the Earth's surface leads to an increase especially of the near-surface density induced signal, e.g. from topography or local structures, which is not necessarily desirable if one wants to do lithospheric modeling. On the other hand, the field at 10 km height better reflects the near-surface geology. For geological mapping

in unknown areas, it can be useful to use the downward continued gradients and use the total horizontal gradient and vertical gradient for geological imaging. Similar analysis can be performed using EGM2008, but for this model one has to be aware of the heterogeneous data sources, which locally might be based on fill-in data (see also Fig. 2). All in all, downward continuation may seem more natural because signal is amplified, but has the disadvantage of amplifying noise and omission error. If the GOCE data are therefore not amended by other data with high frequency content, downward continuation may not be optimal (depending on the

Table 1

Signal and error RMS for the vertical gravity gradient from GOCO03S up to spherical harmonic degree and order 225 and 250 at different heights. The numbers are given for the Arabian Peninsula shown in Fig. 3. The omission error is a global value and was computed using the Tschefferning/Rapp degree variances from $L=251$ and $L=226$ up to $L=100,000$ (Tschefferning and Rapp, 1974).

	$h = 0 \text{ km}$		$h = 10 \text{ km}$		$h = 260 \text{ km}$	
	$L = 250$	$L = 225$	$L = 250$	$L = 225$	$L = 250$	$L = 225$
Signal RMS T_{ZZ}	5.27 E	5.12 E	4.28 E	4.08 E	0.31 E	0.31 E
Predicted error T_{ZZ}	2.28 E	1.25 E	1.58 E	0.89 E	0.4 mE	0.4 mE
SNR	2.31	4.10	2.65	4.58	775	775
Omission error	83.45 E	83.48 E	7.96 E	8.12 E	0.1 mE	0.2 mE

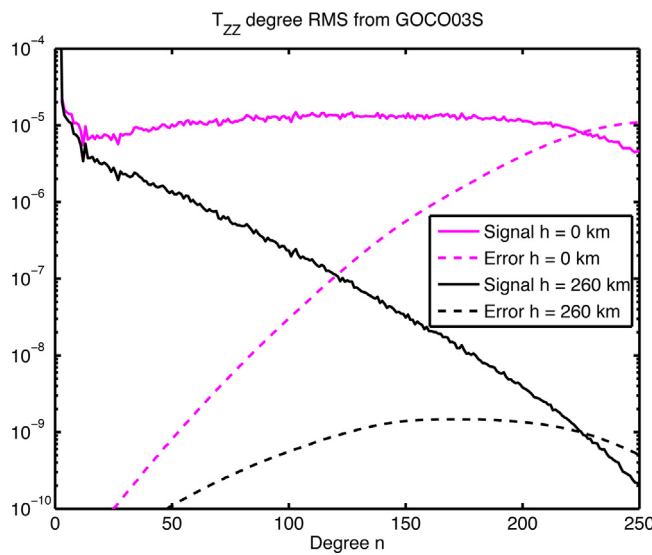


Fig. 4. Degree RMS from GOCO03S for the vertical gravity gradient. The solid lines represent the signal degree RMS, the dashed lines the error degree RMS. Signal and error at satellite height are given in black, at the Earth's surface in purple. The degree where signal equals error is around $L=225$ in both cases. From degrees $L=50$ to $L=250$ the error curve is relatively flat at satellite height, whereas the signal decays exponentially with degree. At ground level it is the other way around: the signal degree RMS is relatively flat, whereas the errors show a more or less exponential increase with degree. (For interpretation of the references to color in this figure legend, the reader is referred to the web version of the article.)

application) and it may be better to leave the data at mean satellite altitude.

2.3. Gravity gradient grids for geophysical studies

We computed gravity gradient grids at mean satellite altitude using a regional modeling approach (Schmidt et al., 2007). Fig. 5 shows exemplarily grids at 270 km altitude for the North-East Atlantic study area. Displayed are the second derivatives of the disturbing gravitational potential T relative to the reference ellipsoid WGS84. We applied a regional modeling approach using spherical basis functions based on series expansions in terms of Legendre polynomials up to degree and order 255. The related unknown scaling coefficients are estimated by relative weighting of the GOCE observations, which have been reduced by the background model GOCO03S, using variance components. The less accurate gradients V_{XY} and V_{YZ} thus get lower weights. Rotating the observation equations for the analysis process into the GRF enables the use of the original GOCE gravity gradients. In the synthesis we multiply the estimated coefficients with Blackman scaling functions and locate them finally in the LNOF on a regular grid at mean orbit height. The average resolution is 0.7° and depends on the maximum degree of the series expansion. The 6 different output grids in the tensor arrangement in Fig. 5 show spatial dependent gravity gradients. The T_{ZZ} component pointing in radial direction down to the Earth contains the largest signal with magnitudes of $\pm 0.5 \text{ E}$ ($\text{E} = 10^{-9} \text{ s}^{-2}$). The variations in the North directed T_{XX} and West directed T_{YY} components are smaller and opposite so that the sum of the diagonal elements (trace criterion) is approximately zero and thus fulfills the Laplace equation. A comparison with gradient

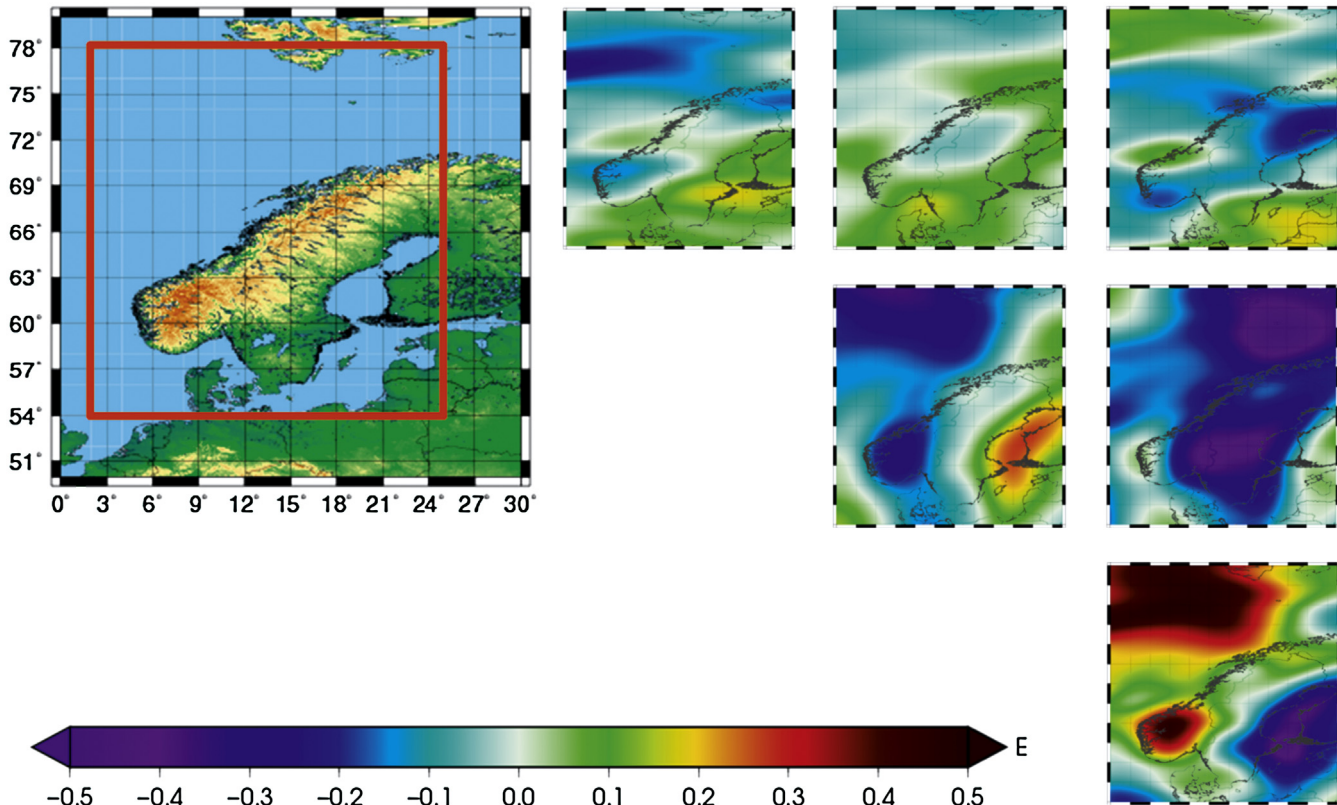


Fig. 5. Gravity gradient grids of the second derivatives of disturbing potential in the LNOF at a mean orbit height of 270 km in the North-East Atlantic Margin. Top row: T_{XX} , T_{XY} , T_{XZ} ; middle row: T_{YY} , T_{YZ} , bottom row: T_{ZZ} . The red rectangle in the map on the top left indicates the region where the gradients were computed. (For interpretation of the references to color in this figure legend, the reader is referred to the web version of the article.)

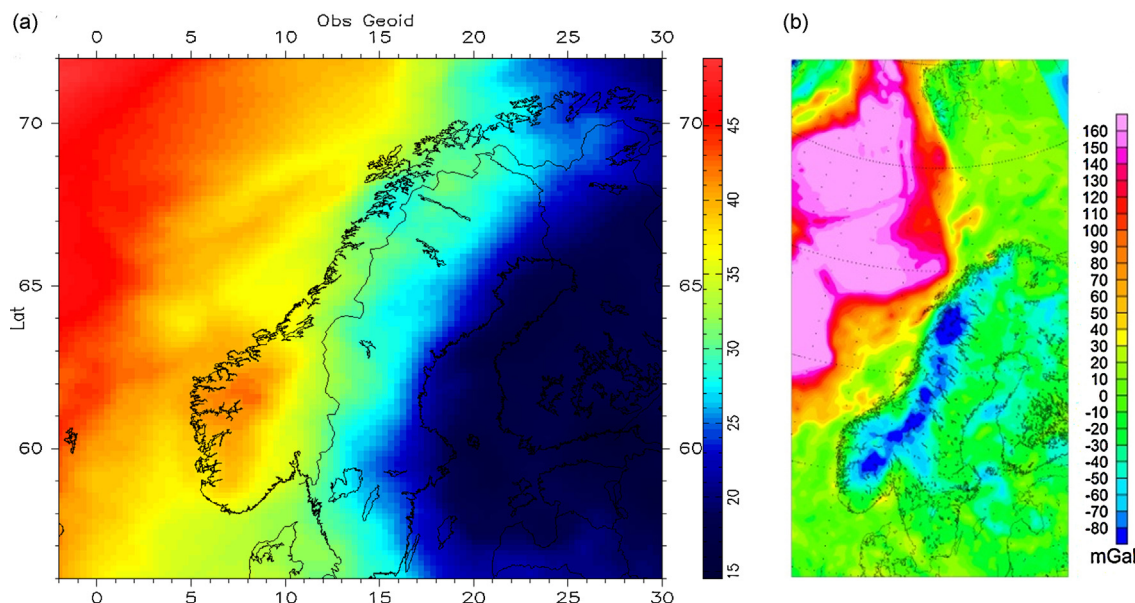


Fig. 6. (a) Geoid (m) with degree and order > 11 and (b) Bouguer anomaly (mGal).

grids obtained from the global spherical harmonic model GOCO03s up to degree and order 250 shows differences between ± 0.5 mE. Thus our regional approximation fits very well to the global model considering errors due to smoothing, interpolation and edge effects.

The gravity gradient grids are given above the Earth's surface in coordinates with respect to a reference ellipsoid. It is quite common, however, that geophysical modeling software use planar approximation with a different north and up direction. Bouman et al. (2013) have shown that these orientation differences should not be neglected to avoid systematic errors, and derived an algorithm to rotate from the LNOF to the planar model reference frame (MRF). They also show that if topographic reduction is to be applied, the computation of this reduction in planar approximation may lead to systematic errors and spherical computations are required. Thus the GOCE gradients in the LNOF should be reduced for topography and thereafter rotated to the MRF. Beforehand, one may reduce the gradients for the long wavelength contribution, for example by removing all signal below spherical harmonic degree and order 10 using a global gravity field model.

3. GOCE gradients for the North-East Atlantic margin

The North-East Atlantic region is well studied in terms of regional geophysics. This makes it an ideal area to analyze the use of GOCE gravity gradients in addition to other geophysical data sets. We will only use the field at mean satellite height (270 km), which is, for the reasons discussed before, best suited for forward and inverse modeling.

3.1. Geoid, gravity and gravity gradients for the NE Atlantic

In the North-East Atlantic region, both the geoid and gravity field show a strong regional trend (Fig. 6, Ebbing and Olesen, 2005). This trend is related to the transition from oceanic to continental domain and additionally explained by the mid-Atlantic ridge and the vicinity to the Iceland hotspot, which are associated with a strong thermal gradient in the asthenosphere and lithosphere. Subtracting the long-wavelength (spherical harmonic degrees < 11) does in theory suppress the sub-lithospheric signal (e.g. Bowin, 1991, 2000), but the trend persists due to the change in lithospheric thickness and its thermal state. As a consequence modeling of the

crust is affected by how the long-wavelength signal is treated, e.g. suppressed by wavelength filtering or included by modeling of the base lithosphere.

Gravity gradients at satellite height have a different characteristic and might be better suited to analyze crustal thickness. Due to the height of the observations, the gradients do in first order reflect the large-scale regional tectonic setting and not local structures. We will here analyze to which part of the lithosphere the gravity gradients signal is sensitive.

3.2. Sensitivity of GOCE data to lithospheric density structure

To study the sensitivity of satellite gradients, we need a 3D lithospheric model with sufficient detail and resolution. We use a model based on a variety of input data sets, which have been compiled previously (Table 2 and Fig. 7). The 3D model is optimized for the gravity field and has a residual of in general < 15 mGal ($1 \text{ mGal} = 10^{-5} \text{ m/s}^2$) for the entire study area, which is a satisfying fit for such a regional model. Table 2 shows the model set-up and the main references for the geometry of the 3D model.

To analyze the sensitivity of satellite gravity gradients to the lithosphere, we (1) compile a 3D subsurface model, (2) subtract a background model, and (3) compute the effects of different depth slices of the model. These steps are briefly discussed below.

(1) Initial 3D density model of the lithosphere

The initial 3D model extends to 300 km depth with a horizontal resolution of $10 \text{ km} \times 10 \text{ km}$. The model is defined layer-wise and is optimized for surface gravity data in planar approximation. Here, the initial model is transformed to a spherical block model in geographical coordinates with a resolution of 0.1° in east and north direction, and a varying vertical resolution. We extend the study area by 5° in all directions to avoid edge effects in the later calculations.

The depth slices are selected with respect to the depths and uncertainties of the individual model geometries. For the upper 10 km depth slices of 2.5 km are used to have a regional, but realistic representation of the top basement. From 10 km to 50 km depth 5 km thick depth slices are used. This is reasonable with respect to the uncertainties of seismic crustal thickness estimates which are at least ± 2 km (Ebbing et al., 2012). From

Table 2

Model set-up and main references for the geometry of the 3D model. See text for details on density functions.

Layer	Model density (kg/m^3)	Reference
Topography	2670	ETOPO1 (Amante and Eakins, 2009)
Water	1030	ETOPO1 (Amante and Eakins, 2009)
Sediments	Density function	Ebbing and Olesen (2010)
Upper crust	2700	Ebbing and Olesen (2010) and Ebbing et al. (2012)
Middle crust	2850	Ebbing and Olesen (2010) and Ebbing et al. (2012)
Lower crust	2950	Ebbing and Olesen (2010) and Ebbing et al. (2012)
High density lower crust	3100	Ebbing et al. (2012)
Moho	Density function	Grad and Tiira (2009)
Base lithosphere	3200	Artemieva (2006)

50 km to 300 km depth the gravity gradients are calculated for depth slices of 25 km thickness. The thickness of the depth slices is reasonable compared with the resolution of seismic tomography (>30 km) and considering the resolution of the input data. The base lithosphere by Artemieva (2006) is for example given with a lateral resolution of 5–5 degrees (Fig. 9).

(2) Subtraction of a reference/background model

Gravity anomalies are sensitive to relative density contrasts, not absolute densities. To study the relative effect of each layer, we calculate a mean density for each layer. The mean density is increasing with depth and corresponds to a normal Earth reference model. The choice of the mean density does have little effect on the gravity gradients, and we subtract the mean layer density to obtain relative density contrasts.

(3) Forward calculation of gravity gradients for depth slices

In the last step, we forward calculate the gravity gradients for the spherical geometry with the software Tesseroids (Uieda et al., 2011). The original rectangular prisms are transferred to spherical prisms (tesseroids) with identical geographical extension, but changing volume depending on distance to the center of the Earth. The calculation in tesseroids is computationally more demanding than for simple prisms. But by using tesseroids we can neglect issues related to tensor rotation and, more importantly, incorrect distance between source masses and observation point. The numerical noise of the calculations has been evaluated using the Laplace equation, and resulted in values several orders of magnitudes smaller than the error of the GOCE measurements.

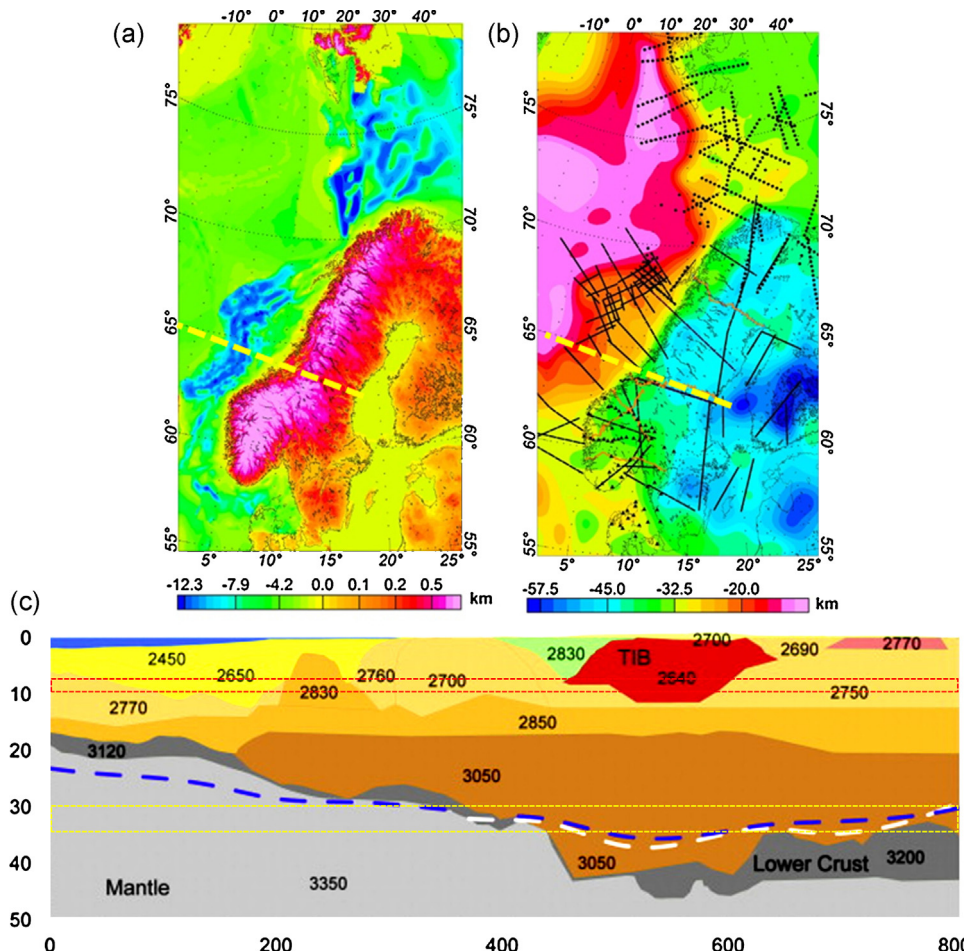


Fig. 7. Key horizons of 3D lithospheric model. (a) Top basement (after Ebbing and Olesen, 2010), (b) Moho depth, (c) crustal cross section through 3D model (Ebbing et al., 2012); depth and distance along cross section in km. Location of profile is indicated by yellow line in (a) and (b). Yellow and red box in (c) indicate depth slices for which results are shown in Fig. 8. (For interpretation of the references to color in this figure legend, the reader is referred to the web version of the article.)

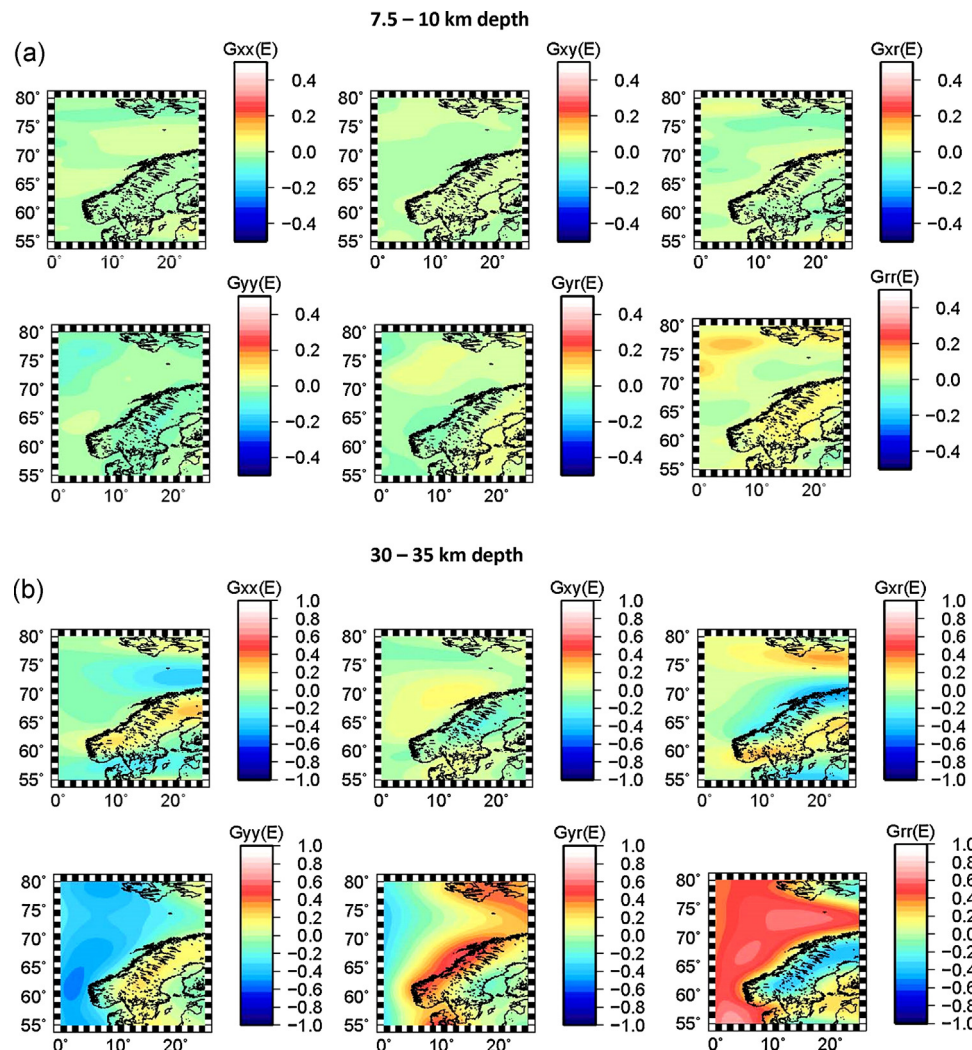


Fig. 8. Calculated gravity gradients at satellite height (270 km) for depth slices at 7.5–10 km and 30–35 km depth. For the complete results from surface to 50 km depth, see Supplementary File 1.

3.2.1. Calculated gravity gradients for the crust

Fig. 8 shows the satellite gravity gradients for two selected depth slices 7.5–10 km depth, and 30–35 km depth (for a complete overview of gravity gradients for depth slices from surface to 200 km depth, see Supplementary File 1). The first depth slice is selected such that it lies within the crust and does not cut the bathymetry or Moho, the second depth slice lies at a typical Moho depth (see Fig. 7c).

The gravity gradients at satellite height for the intra-crustal depth slice show only very small amplitudes of <0.1 E. Only the vertical gradient shows slightly higher amplitude. Even though the crustal density is varying from 2600 kg/m³ to 2850 kg/m³, the results imply that the gravity gradients at satellite height are quite insensitive to intra-crustal density sources, which can nevertheless have quite a large effect on the surface gravity data (e.g. Ebbing et al., 2012).

The second depth slice crosses the Moho and shows a quite high signal. The vertical gradient has an amplitude of >1 E, and the other components have amplitudes in the order of >0.5 E (Fig. 8, bottom). The results show that all components are highly sensitive to the density contrast between crust and mantle (here 200 kg/m³). The different characteristics of the gradient components could be further exploited by forward and inverse modeling of crustal thickness.

The calculations for crustal depth slices reveal that only the interfaces with large density contrasts (topography/bathymetry and Moho) have a distinct signal in the gravity gradients at satellite height.

3.2.2. Upper mantle sensitivity

Typically, uppermost mantle densities are in the range of 3300–3400 kg/m³ and for studies on a semi-regional scale a constant density is often chosen. For large-scale modeling areas, which cross over different tectonic domains (e.g. from the North-Atlantic plate into the passive continental margin and into the Fennoscandian shield) this approach is too simplistic and lateral varying densities according to the thermal state of the lithosphere should be applied. Therefore, we apply to the lithospheric mantle a temperature-dependent density gradient (Fig. 9a).

The gradient is calculated with (e.g. Fullea et al., 2007):

$$\rho_m(T) = \rho_{m0}[1 - \alpha_v(T_L - T_0)]$$

where ρ_m is the in situ density, ρ_{m0} is the normal mantle density at the base lithosphere, T_0 is the temperature at the base lithosphere, T_L is the in situ temperature, which can be estimated from geothermal gradients and α_v is the adiabatic temperature coefficient.

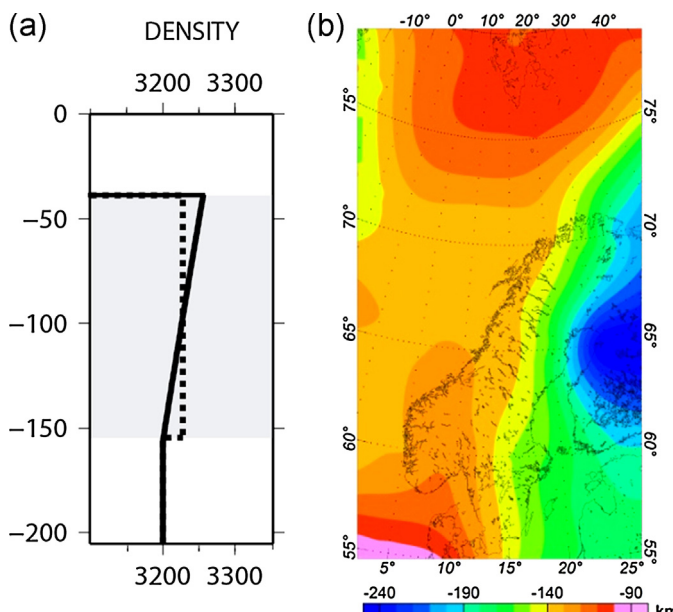


Fig. 9. (a) Graph showing depth dependent mantle densities (calculated with $\rho_{m0} = 3200 \text{ kg/m}^3$, $\alpha_v = 3E-5 \text{ K}^{-1}$ and $T_L = 1300^\circ\text{C}$). Gray area indicates lithospheric mantle and (b) base lithosphere after Artemieva (2006).

Fig. 10 shows that the related gravity gradients signal diminishes rapidly with depth, and most signal stems from above 150 km. But even for these depth ranges a rapid change is visible, and already beneath 75 km depth it would be possibly that local, compositionally caused density variations could be observed. Notably, the gradient signal at satellite height has a high sensitivity

to the uppermost mantle, where seismic tomography has an imaging problem and often omits results (e.g. Levshin et al., 2007).

For all tensor components the signal rapidly diminishes with depths (see Supplementary File 1). This is also expressed by the rotational invariants I1 and I2 in Fig. 10. Gradients are dependent on the orientation of the coordinate system, but invariants have the advantage to be independent of the coordinate system (Pedersen and Rasmussen, 1990). In comparison with the vertical gradient, the invariants have a higher sensitivity to shallower sources. In summary, the satellite gradients have a depth sensitivity which makes them well suited to the study the upper mantle density structure and to verify density distributions based on seismic tomography.

3.3. Discussion

In the model set-up all geometries and densities are associated with a given uncertainty. This implies that in gravity modeling a small change in crustal thickness can be compensated by a change in sedimentary thickness, leading to a similar gravity effect as in the initial model. If the gravity gradients are used, changes in crustal thickness cannot be as easily compensated as the sensitivity to intra-crustal densities is very low.

On the other hand, satellite gravity gradients are quite sensitive to the upper mantle density distribution. In our example, we neglected the effect of pressure and composition on the densities, but this is typically a minor effect compared with temperature. The thermal field depends on the base lithosphere, which is determined with large uncertainties. But the sensitivity study shows that the gradients are less sensitive to the overall lithospheric thickness, but more to lateral varying densities down to 150 km depth. It is therefore reasonable to assume that compositional changes in the upper mantle can be better defined when satellite gradients are used in addition to conventional gravity data and with a reasonable

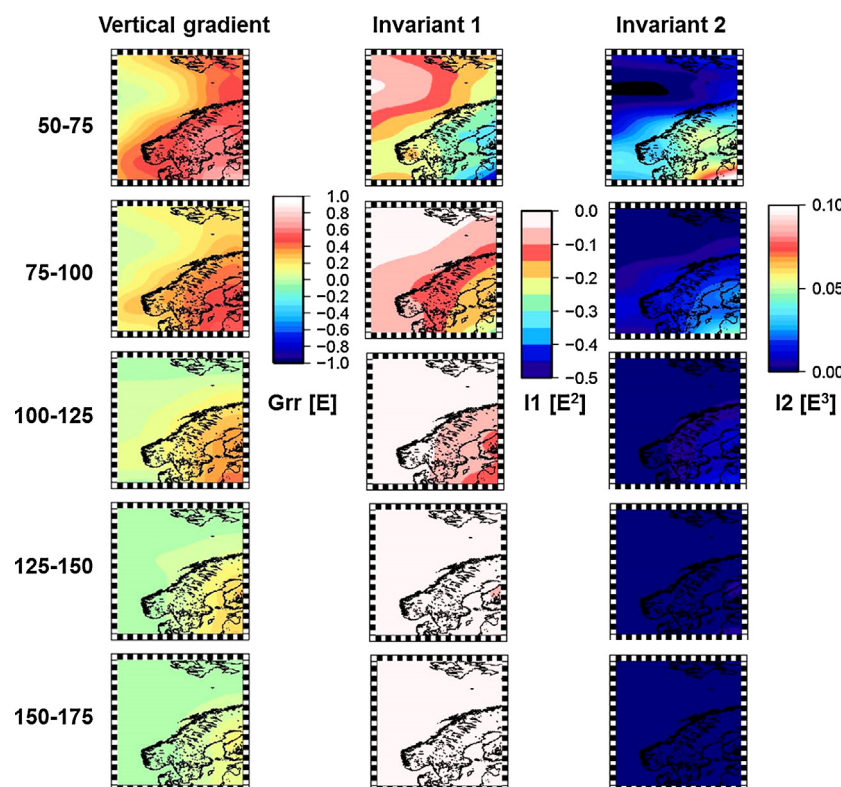


Fig. 10. Sensitivity to upper mantle density distribution: the vertical gravity gradients and rotational invariants, I1 and I2, were calculated at satellite height (270 km) for 25 km thick depth slices from 50 km to 175 km depth. For other tensor components, please see Supplementary File 1.

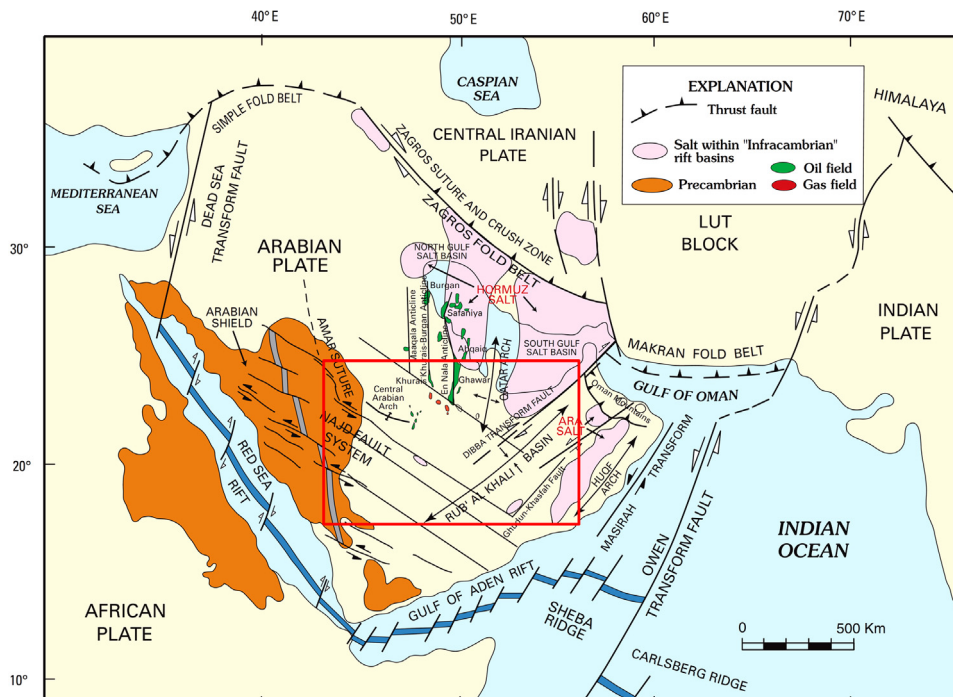


Fig. 11. Arabian Plate showing general tectonic and structural features (Pollastro, 2003) and the study area (red rectangle). (For interpretation of the references to color in this figure legend, the reader is referred to the web version of the article.)

Source: U.S. Geological Survey, Department of the Interior/USGS, reproduced by permission of GeoArabia.

well-defined crustal setting. Especially the use of the invariants in inverse modeling might be promising to pursue.

4. GOCE gradients for the Rub'al-Khali

We present a case-study for the Rub'al-Khali region that illustrates a potential application of the GOCE data in geophysical exploration. Accumulation of hydrocarbons (oil and gas) in the subsurface depends on several factors, one of which is the maturity of the source rock. The maturity of the source rock is the ability of organic rich layers (source rocks) to produce hydrocarbon and is dependent on the amount of heat that is available in the basin. The amount of heat in the basin is controlled by the thermal gradient in the subsurface which is normally defined by the heat flow in the basin. Heat flow is influenced by the deeper structures in the basin, such as the depth to Moho and the lithospheric thickness. A better understanding of the deep structures in a basin can help to improve models of the heat flow and therefore improve the prediction of the source rock maturity and hydrocarbon accumulations (Barker, 1996; Beardmore and Cull, 2001; Allen and Allen, 2005; Hantschel and Kauerauf, 2009). Since GOCE gradient data have the potential to constrain the crustal thickness (Moho depth), it could be used to calculate the heat flow in areas where limited data is available. The Rub'al-Khali basin, central Saudi Arabia (Fig. 11), is selected as a case study to demonstrate how a crustal model derived from GOCE data is used to model heat flow and maturity. The implemented workflow is illustrated in Fig. 12.

4.1. Data availability and initial geological model

For the interpretation of the GOCE data and heat flow modeling an initial 3D geological model is constructed for the study area based on available public and literature data (Fig. 14). The model consists of a top crystalline basement (Konert et al., 2001; Stern and Johnson, 2010) and 9 sedimentary units stretching from the Cenozoic to the Ordovician (Peterson and Wilson, 1986; Christian,

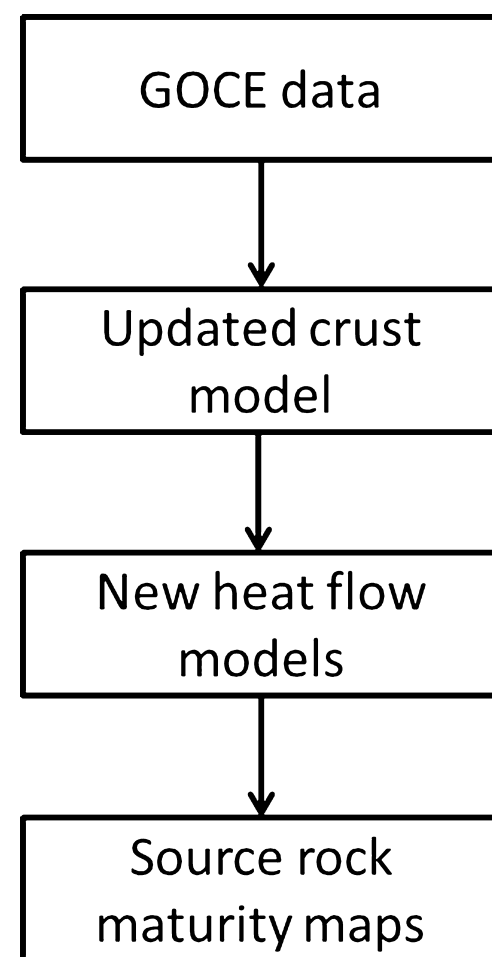


Fig. 12. Workflow showing the use of gravity data for calculating maturity maps of the main source rocks.

1997; Al-Jallal, 1995; Pollastro, 2003; Alsharhan and Nairn, 1997; Edgell, 1976; Mahmoud et al., 1992; Senalp and Al-Duaiji, 2001). ETOPO1 is used to represent the topography and bathymetry in the region (Amante and Eakins, 2009). The depth to Moho interface, calculated from receiver function analysis, is available at the location of a number of seismic stations in the area (Al-Lazki et al., 2002; Al-Damegh et al., 2005). These values are used to calibrate the modeled Moho depth based on GOCE data. Depth to the top of the asthenosphere is derived from the lithospheric thermal model given by Artemieva (2006).

4.2. Updated GOCE-based Moho model

The GOCE vertical gradient component at satellite altitude (~260 km) was used to obtain an updated Moho model of the Rub'al-Khali basin. It was not possible to carry out a full inversion of the GOCE gradients. However, the modeling steps carried out do show the beneficial value of the GOCE gradients for obtaining an improved Moho model. One of the main problems in the area is to assign the general change in the gravity gradients and the Bouguer gravity anomaly to either the base of the lithosphere, the Moho or the general trend in the top basement. There is a certain freedom in exchanging the part of the field from one interface to the other. Most uncertain in this area is the position of the Moho, whereas the trend of the basement seems to be fairly well known from drillings and the trend in the base lithosphere is also assumed to be known. The workflow is shown in Fig. 13. First of all, the data are corrected for the mass of the topography using the ETOPO1 model. The corrections are calculated as above using the software Tesseroids (Uieda et al., 2011). In this study we used 2300 kg/m³ for the surface density – to comply with the density used for the Bouguer anomaly data that are also available for the area – and 1030 kg/m³ for water density. Then the effect of the top asthenosphere and lower lithospheric layers is calculated and subtracted from the gradient data. The gravity signal of the top basement is calculated at satellite altitude as well, using a density contrast of 300 kg/m³. We designed empirical formulae that link the residual data to the depth of the Moho. It was done in two steps: first G_{zz} was converted to the depth of the Moho (M_0). In a second step the difference between the data and the response of M_0 was used to

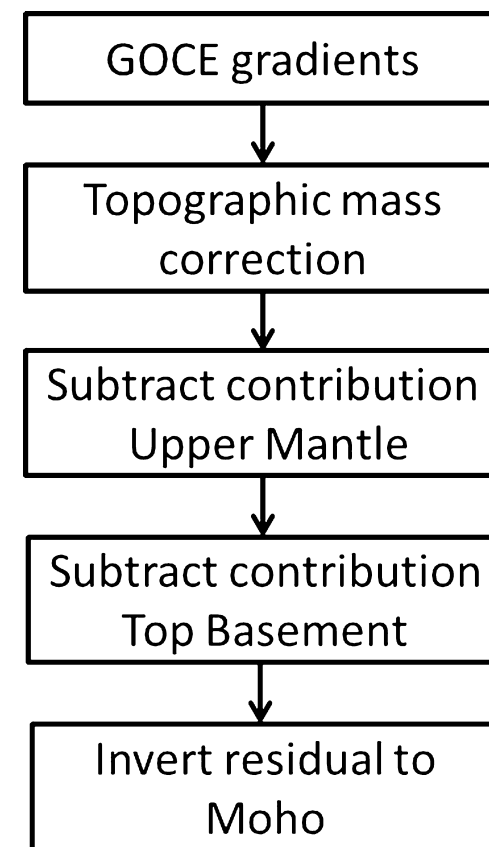


Fig. 13. Workflow showing the use of gravity data for calculating an updated Moho.

adjust the depth of the Moho (M_1). The formula for calculating and adjusting the depth of the Moho is interactively lightly constrained at the location of seismic stations. The response of this new Moho M_1 is also depicted in Fig. 15. It is seen that the G_{zz} data are similar to the model response as this was the data that was used to build the model. However, the figure shows that the similarity between the data and the model response for the other components is also

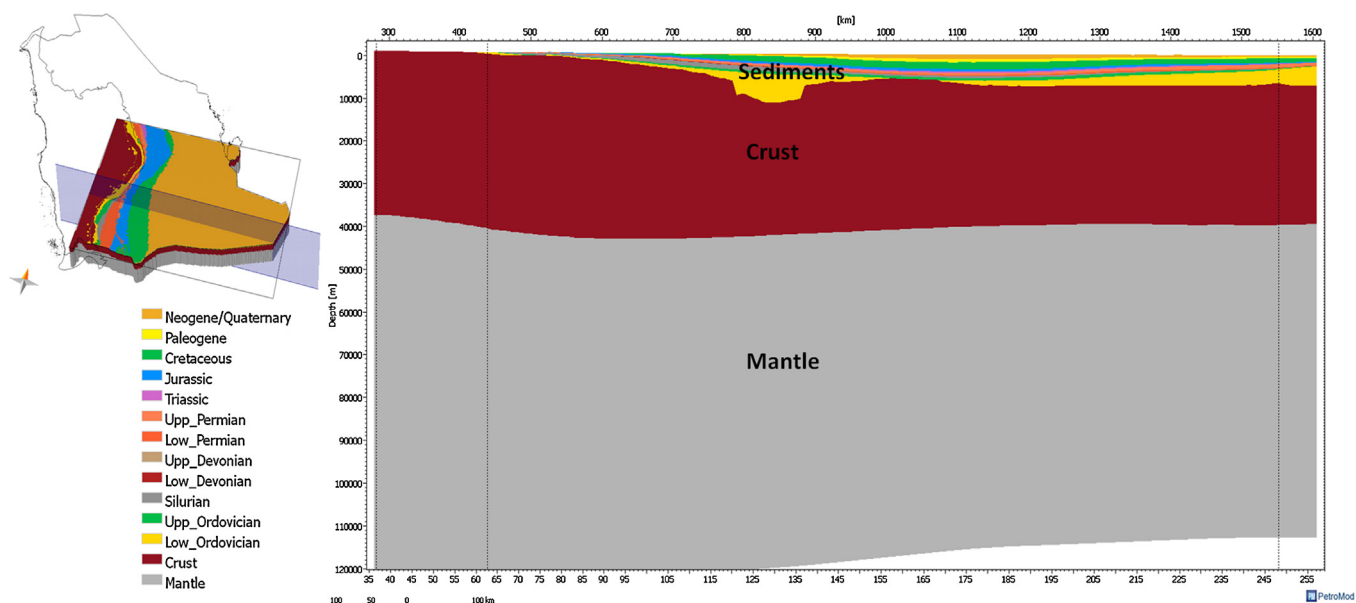


Fig. 14. The constructed 3D geological model for the Rub'al-Khali region (see the text for details). The model is used for gravity interpretation, heat flow and source rock maturity modeling.

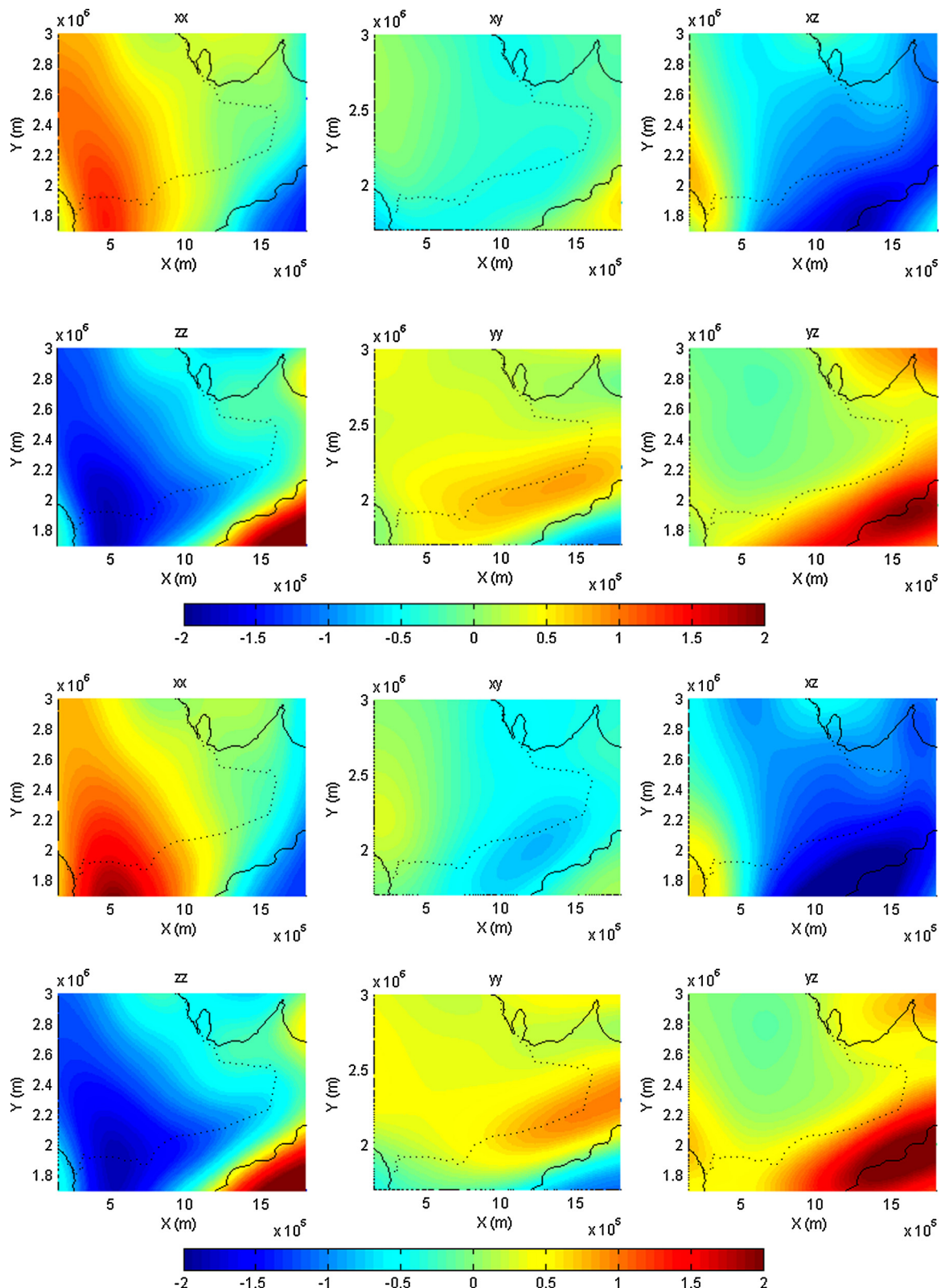


Fig. 15. Reduced GOCE gravity gradient data (E) related to Moho (top panel). Gravity gradients from model with updated Moho based on GOCE data (lower panel).

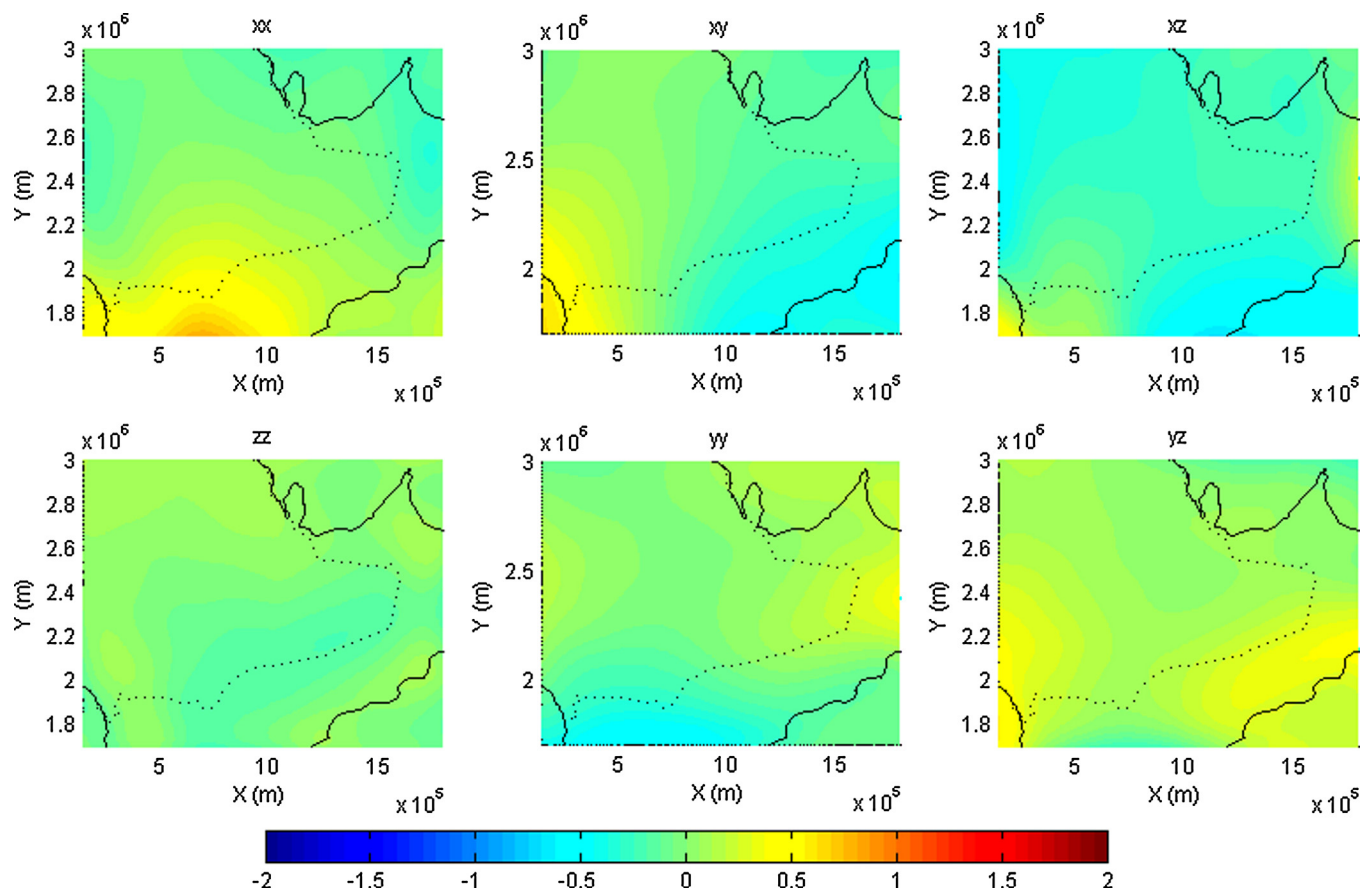


Fig. 16. Difference in E between reduced GOCE gradients and modeled gradients from Fig. 15.

reasonable. Residuals are depicted in Fig. 16. The residuals for the other components range mostly from -0.5 E to 0.5 E , for some components (G_{XX} and G_{XY}) in some areas the residual is larger, but were not analyzed in more detail at this stage.

A comparison between the modeled Moho based on GOCE gradients and the Moho depths derived from seismic stations

(Al-Damegh et al., 2005) shows that the differences are in the range of 5 km at the location of the stations (Fig. 17). The differences are generally within the uncertainty ranges of the measured depths at the seismic stations.

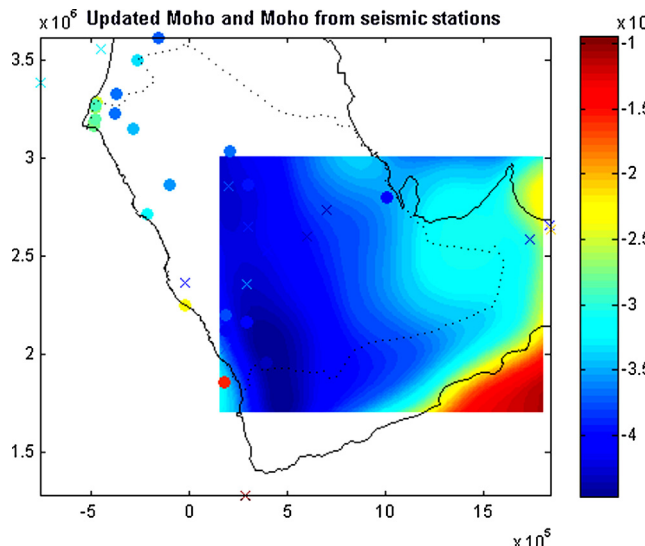


Fig. 17. Modeled top Moho (m) in the Rub'al-Khali basin based on interpretation of GOCE gradient data. Modeled depths are comparable with the measured depths at the locations of seismic stations (colored dots). (For interpretation of the references to color in this figure legend, the reader is referred to the web version of the article.)

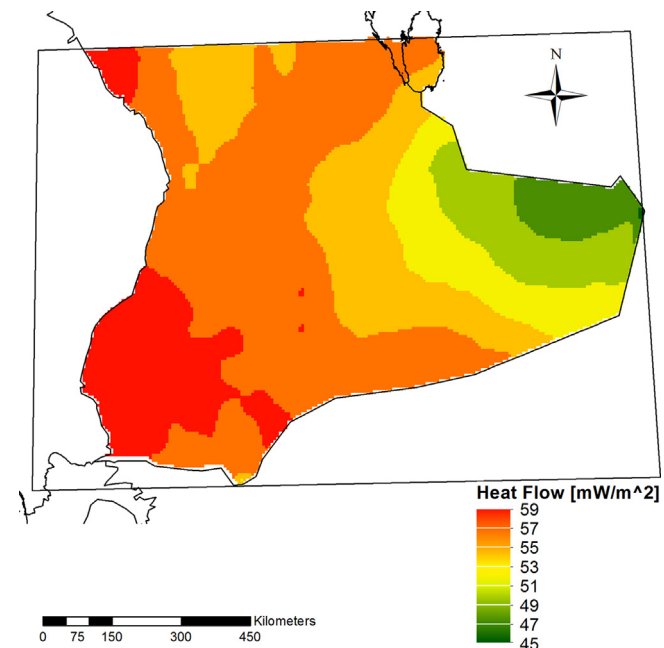


Fig. 18. Modeled heat flow (mW/m^2) in the Rub'al-Khali basin using the GOCE-based Moho.

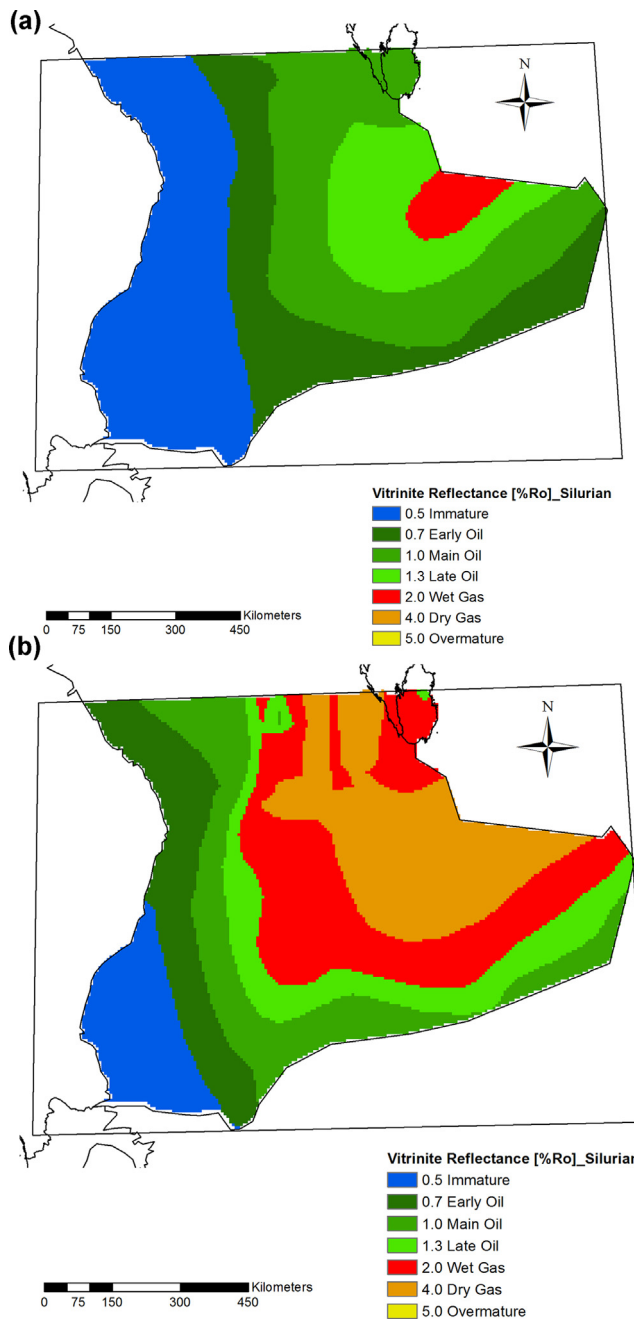


Fig. 19. Modeled maturity of main source rocks in the Rub'al-Khali basin (top: Silurian Source Rock; bottom: Jurassic Source Rock). The predicted maturity is based on the modeled heat flow (Fig. 18).

4.3. Updated heat flow model

The thickness of the crust (Moho depth) influences the heat flow mainly through the amount of heat that the crust produces by the radiogenic elements. Thicker crust would imply higher basal heat flow from the crust for a constant lithospheric thickness. The new Moho depth is incorporated in the initial geological model to calculate the heat flow in the basin. We use a tectonic model that reconstructs the crustal and lithospheric stretching over the geological history of the basin. The stretching of the crust is calculated from the tectonic subsidence of the basin which is modeled through backstripping of the burial history in the basin (Van Wees et al., 2009; Allen and Allen, 2005).

Fig. 18 shows the modeled heat flow in the Rub'al-Khali basin using the GOCE-based Moho. The modeled present-day heat flow ranges from 58 mW/m² in the south-west to ca. 52 mW/m² in the east. The general trend of heat flow variations reflects the trend of the Moho in the area. The short-wavelength variations are more correlated to the variations in sediment thicknesses and depth to top basement.

The modeled present day maturity of the two main source rocks in the region (Silurian and Jurassic) is indicated in **Fig. 19**. The modeled maturity maps show that the basin is still capable of hydrocarbon generation and therefore is prospective. The maturity models are generally consistent with known source rock maturity trends in the surrounding areas (Milner, 1998; Abu-Ali et al., 1999).

The modeled heat flow and source rock maturity are comparable with what is observed in the vicinity of the basin. This indicates that the geological model (including the new Moho) is reasonable at least in the areas where observations are available.

4.4. Discussion

The workflow implemented to process and interpret GOCE gradient data considers the major main density contrasts interfaces such as the top basement, the Moho and the base lithosphere. The compensation for the top basement density contrast is carried out even though gravity gradients are less sensitive to intra-crustal densities.

The modeled depth of the Moho is generally similar to the values derived from seismic stations. However, some discrepancy is observed with a few stations where the modeled depth falls outside the error margin of the seismic observations. As in the use of normal gravity data, inverse and forward modeling would benefit from using the seismic information as bounding constraints during the calculations.

The gradient components of the inverted Moho depth provide a good fit with 4 out of 6 of the measured gradient components at satellite altitude. The analysis in Section 3 has shown that the depth sensitivity of the tensor components is variable. This might imply that the mismatch with the G_{XX} and G_{XY} component can be used to update the density model. For geological exploration of intra-crustal structures the primary targets are usually basins and top basement topography. These shallow structures can be identified better by complementing GOCE gradients with, for example, terrestrial gravity data.

5. Conclusions

We studied how GOCE gravity gradients can improve modeling of the Earth's lithosphere and conclude that these new satellite gravity data are a useful additional dataset that amends more common data, such as gravity and seismic. The original GOCE data are not directly used, but we predict gravity gradients in a grid at mean orbital altitude in a regional gravity field estimation approach. The advantage over the original data is that errors average out and that one does not have to handle gravity gradients with very different error characteristics in a rotating instrument frame at varying heights. The downward continuation of the gradients to grids close to the Earth's surface enhances signal and better reflects the near-surface geology, which may be an advantage for geological mapping in unknown areas. Nevertheless, downward continuation has the disadvantage of amplifying noise and omission errors especially because of topography induced signal, which is a disadvantage for forward and inverse modeling. Therefore we recommend using the field at mean satellite altitude.

Our calculations for crustal depth slices reveal that interfaces with large density contrasts, such as topography/bathymetry and

Moho, have a distinct signal in the gravity gradients. On the other hand, the satellite gravity gradients are quite insensitive to intra-crustal density sources, which can have quite a large effect on surface gravity data. The satellite gradients have a depth sensitivity which makes them well suited to the study of the upper mantle density structure and to verify and complement density distributions based on seismic tomography, which has an imaging problem for the upper mantle. The use of gravity gradient invariants in inverse modeling might be promising to pursue.

Because of the sensitivity of the GOCE gravity gradients to interfaces with large density contrasts, these data can be used to improve the Moho model in not so well surveyed areas. The updated Moho model for the Rub'al-Khali gives a good fit to four of the six gradients, whereas the fit is not so well for the two other gradients. An independent validation with Moho depths from a few available seismic stations shows that the differences are generally within the depth uncertainty ranges. The updated Moho model was used to update the heat flow model and source rock maturity maps. The latter are generally consistent with known source-rock maturity trends in the surroundings of the Rub'al-Khali. We therefore conclude that for frontier areas, where not much data are available, GOCE gradients can be useful to map crustal thickness and deep regional structures. In combination with other data, heat flow can be modeled which is essential for assessment of basin maturity.

Acknowledgements

This work has been done in the framework of the ESA sponsored GOCE+ GeoExplore study as part of ESA's Support to Science Element (STSE). We thank the reviewers Hajo Götze and Zdeněk Martinec for their comments, which helped to improve the manuscript.

Appendix A. Supplementary data

Supplementary data associated with this article can be found, in the online version, at <http://dx.doi.org/10.1016/j.jag.2013.11.001>.

References

- Abu-Ali, M.A., Rudkiewicz, J.L.L., McGillivray, J.G., Behar, F., 1999. Paleozoic petroleum system of Central Saudi Arabia. *GeoArabia* 4, 321–336.
- Al-Damegh, K., Sandvol, E., Barazangi, M., 2005. Crustal structure of the Arabian Plate: new constraints from the analysis of teleseismic receiver functions. *Earth Planet. Sci. Lett.* 231, 177–196.
- Al-Jallal, A.I., 1995. The Khuff formation—its reservoir potential in Saudi Arabia and other Gulf countries. In: Al-Husseini, M.I. (Ed.), *Geo-94, Middle East Petroleum Geosciences Conference*. Gulf Petrolink, Manama.
- Al-Lazki, A.I., Seber, D., Sandvol, E., Barazangi, M., 2002. A crustal transect across the Oman Mountains of the eastern margin of Arabia. *GeoArabia* 7, 47–78.
- Allen, P.A., Allen, J.R., 2005. *Basin Analysis, Principles and Applications*, second ed. Wiley-Blackwell, Hoboken, New Jersey, 500 pp.
- Alsharhan, A.S., Nairn, A.E.M., 1997. *Sedimentary Basins and Petroleum Geology of the Middle East*. Elsevier, Amsterdam, 878 pp.
- Amante, C., Eakins, B.W., 2009. ETOPO1 1 Arc-Minute Global Relief Model: Procedures, Data Sources and Analysis. NOAA Technical Memorandum NESDIS NGDC-24, 19 pp.
- Artemieva, I.M., 2006. Global $1^\circ \times 1^\circ$ thermal model TC1 for the continental lithosphere: implications for lithosphere secular evolution. *Tectonophysics* 416, 245–277.
- Barker, C., 1996. *Thermal Modeling of Petroleum Generation: Theory and Application*. Elsevier Science, Amsterdam, 415 pp.
- Beardmore, G.R., Cull, J.P., 2001. *Crustal Heat Flow*. Cambridge University Press, Cambridge.
- Bouman, J., Fuchs, M.J., 2012. GOCE gravity gradients versus GOCE gravity field models. *Geophys. J. Int.* 189, 846–850, <http://dx.doi.org/10.1111/j.1365-246X.2012.05428.x>.
- Bouman, J., Rispen, S., Gruber, T., Koop, R., Schrama, E., Visser, P., Tscherning, C.C., Veicherts, M., 2009. Preprocessing of gravity gradients at the GOCE high-level processing facility. *J. Geod.* 83, 659–678, <http://dx.doi.org/10.1007/s00190-008-0279-9>.
- Bouman, J., Fiorot, S., Fuchs, M., Gruber, T., Schrama, E., Tscherning, C.C., Veicherts, M., Visser, P., 2011. GOCE gravitational gradients along the orbit. *J. Geod.* 85, 791–805, <http://dx.doi.org/10.1007/s00190-011-0464-0>.
- Bouman, J., Ebbing, J., Fuchs, M., 2013. Reference frame transformation of satellite gravity gradients and topographic mass reduction. *J. Geophys. Res.* 118, 759–774, <http://dx.doi.org/10.1029/2012JB009747>.
- Bowin, C., 1991. The Earth's gravity-field and plate-tectonics. *Tectonophysics* 187, 69–89.
- Bowin, C., 2000. Mass anomalies and the structure of the Earth. *Phys. Chem. Earth A* 25, 343–353.
- Christian, L., 1997. Cretaceous surface geology of the Middle East Region. *GeoArabia* 2, 239–256.
- Ebbing, J., Olesen, O., 2005. The Northern and Southern Scandes – structural differences revealed by an analysis of gravity anomalies, the geoid and regional isostasy. *Tectonophysics* 411, 73–87.
- Ebbing, J., Olesen, O., 2010. New compilation of top basement and basement thickness for the Norwegian continental shelf reveals segmentation of the passive margin system. *Petrol. Geol. Conf. Ser.* 7, 885–897.
- Ebbing, J., England, R.W., Korja, T., Lauritsen, T., Olesen, O., Stratford, W., Weidle, C., 2012. Structure of the Scandes lithosphere from surface to depth. *Tectonophysics*, <http://dx.doi.org/10.1016/j.tecto.2011.03.031>.
- Edgett, H.S., 1976. The Permian system as an oil and gas reservoir in Iran, Iraq and Arabia. In: *2nd Iranian Geol. Symp.*, Tehran, pp. 161–195.
- ESA, 1999. Gravity field and steady-state ocean circulation mission, Reports for mission selection; the four candidate earth explorer core missions, SP-1233(1). ESA.
- Frommknecht, B., Lamarre, D., Bigazzi, A., Meloni, M., Floberghagen, R., 2011. GOCE level 1b data processing. *J. Geod.* 85, 759–775, <http://dx.doi.org/10.1007/s00190-011-0497-4>.
- Fuchs, M.J., Bouman, J., 2011. Rotation of GOCE gravity gradients to local frames. *Geophys. J. Int.* 187, 743–753, <http://dx.doi.org/10.1111/j.1365-246X.2011.05162.x>.
- Fullea, J., Fernández, M., Zeyen, H., Vergés, J., 2007. A rapid method to map the crustal and lithospheric thickness using elevation, geoid anomaly and thermal analysis. Application to the Gibraltar Arc System, Atlas Mountains and adjacent zones. *Tectonophysics* 430, 97–117.
- Grad, M., Tiira, T., ESC Working Group, 2009. The Moho depth map of the European Plate. *Geophys. J. Int.* 176, 279–292.
- Hantschel, T., Kauerauf, A.I., 2009. *Fundamentals of Basin and Petroleum Systems Modeling*. Springer, Berlin, Heidelberg, 476 pp.
- Konert, G., Afifi, A.M., Al-Hajri, S.A., Drost, H.J., 2001. Paleozoic stratigraphy and hydrocarbon habitat of the Arabian Plate. *GeoArabia* 6, 407–442.
- Levshin, A., Schweitzer, J., Weidle, C., Shapiro, N., Ritzwoller, M., 2007. Surface wave tomography of the Barents Sea and surrounding regions. *Geophys. J. Int.* 170, 441–459.
- Mahmoud, M.D., Vaslet, D., Husseini, M.I., 1992. The Lower Silurian Qalibah Formation of Saudi Arabia – an important hydrocarbon source rock. *Am. Assoc. Petrol. Geol. Bull.* 76, 1491–1506.
- Mayer-Gürr, T., Rieser, D., Höck, E., Brockmann, J.M., Schuh, W.D., Krasbutter, I., Kusche, J., Maier, A., Krauss, S., Hausleitner, W., Baur, O., Jäggi, A., Meyer, U., Prange, L., Pail, R., Fecher, T., Gruber, T., 2012. The new combined satellite only model GOCO03s. In: *Poster Presented at the GGHS2012, Venice*.
- Milner, P.A., 1998. Source rock distribution and thermal maturity in the southern Arabian Peninsula. *GeoArabia* 3, 339–356.
- Pail, R., Bruinsma, S., Migliaccio, F., Förste, C., Goiginger, H., Schuh, W.D., Höck, E., Reguzzoni, M., Brockmann, J.M., Abrilovskov, O., Veichert, M., Fecher, T., Mayrhofer, R., Krasbutter, I., Sansö, F., Tscherning, C.C., 2011. First GOCE gravity field models derived by three different approaches. *J. Geod.* 85, 819–843, <http://dx.doi.org/10.1007/s00190-011-0467-x>.
- Pavlis, N.K., Holmes, S.A., Kenyon, S.C., Factor, J.K., 2012. The development and evaluation of the Earth Gravitational Model 2008 (EGM2008). *J. Geophys. Res.* 117, B04406, <http://dx.doi.org/10.1029/2011JB008916>.
- Pedersen, L.B., Rasmussen, T.M., 1990. The gradient tensor of potential field anomalies: some implications on data collection and data processing of maps. *Geophysics* 55, 1558–1566.
- Peterson, J.A., Wilson, J.L., 1986. Petroleum stratigraphy of the northeast Africa–Middle East region. In: *Symposium on the Hydrocarbon Potential of the Intense Thrust Zone, OAPEC, Kuwait, and Ministry of Petroleum and Mineral Resources, U.A.E.*, 14–18 December, Abu Dhabi, pp. 227–330.
- Pollastro, R.M., 2003. *USGS Bulletin 2202-H*, pp. 80.
- Schall, J., Eicker, A., Kusche, J., 2012. Global and regional gravity field models from GOCE data. In: *Presented at the GGHS Symposium, Venice, Italy*.
- Schmidt, M., Fengler, M., Mayer-Gürr, T., Eicker, A., Kusche, J., Sanchez, L., Han, S.C., 2007. Regional gravity modelling in terms of spherical base functions. *J. Geod.* 81, 17–38, <http://dx.doi.org/10.1007/s00190-006-0101-5>.
- Senalp, M., Al-Duajji, A.A., 2001. Qasim formation: Ordovician storm- and tide-dominated shallow marine siliciclastic sequences, Central Saudi Arabia. *GeoArabia* 6 (2), 233–268.
- Stern, R.J., Johnson, P., 2010. Continental lithosphere of the Arabian Plate: a geologic, petrologic, and geophysical synthesis. *Earth Sci. Rev.* 101 (1/2), 29–67.
- Tscherning, C.C., Rapp, R.H., 1974. Closed covariance expressions for gravity anomalies, geoid undulations, and deflections of the vertical implied by anomaly degree

variance models. Rep 355. Department of Geodetic Science, Ohio State University, Columbus.

Uieda, L., Bomfim, E., Braatenberg, C., Molina, E., 2011. Optimal forward calculation method of the Marussi tensor due to a geologic structure at GOCE height. In: Proceedings GOCE User Workshop 2011, ESA SP-696.

Van Wees, J.D., van Bergen, F., David, P., Nepveu, M., Beekman, F., Cloetingh, S., Bonte, D., 2009. Probabilistic tectonic heat flow modeling for basin maturation: assessment methods and applications. In: Verweij, H., Kacewicz, M., Wendebourg, J., Yardley, G., Cloetingh, S., Düppenbecker, S. (Eds.), Thematic Set on Basin Modeling Perspectives. Mar. Petrol. Geol. 26, 536–551.